

Optimized design of tidal current turbine airfoil for water efficiency

Zhiyang Zhang^{a,b,†}, Bo Wu^{a,b}, Yongqing Liang^b, Jiaju Tang^a, Jun Li^b, Weixing Liu^{a,b}, Shaohua Chen^{a,*}, Lin Cui^{c,*†}

^aCollege of Marine Engineering, Jiangsu Ocean University, Lianyungang 222005, China, email: 17206017543@163.com (S.H. Chen)

^bMakarov College of Marine Engineering, Jiangsu Ocean University, Lianyungang 222005, China

^cNational Ocean Technology Center, Tianjin 300112, China, email: cuilin_oceanenergy@126.com (L. Cui)

Received 29 November 2022; Accepted 20 September 2023

ABSTRACT

Based on NACA63816, NACA63815 and NACA63813 airfoils, an airfoil for large hydraulic turbines is designed. The design optimization software iSight was used to establish an airfoil optimization model building on multi-island genetic algorithm, and the computational fluid dynamics numerical simulation approach was applied to analyze the flow field. The lift-to-drag ratio, drag coefficient and maximum thickness T_m at an airfoil angle of attack of 5° are selected as the optimization target parameters to derive the hydrodynamic coefficients of the airfoil. The optimized airfoil lift coefficients increased by 20%/15%/14% and the lift-to-drag ratios rised by 28%/16%/14%.

Keywords: Hydraulic turbine; Multi-island genetic algorithm; Optimization; Lift coefficient; Lift-to-drag ratio

1. Introduction

Hydraulic turbine power generation technology has been widely used due to its advantages of cleanliness and non-pollution. Completely imported foreign technology for trendy turbines is extremely costly [1]. It is worth noting that the oceans have significant renewable energy potential as a source of energy [2]. Inflexibility and financial threats to system functionality stemming from uncertain parameters in heat loads, electrical and cooling loads, electricity prices and renewable energy generation [3]. Diffuser Enhanced Tidal Turbines have been determined and considered to be highly efficient in converting tidal energy and the blades play a key role in converting tidal energy [4]. At present, to increase the overall energy-acquiring power of the horizontal axis tidal energy turbine, the blades are required to be made longer and longer, which imposes higher requirements on the hydrodynamic performance and structural strength of the blades. The hydraulic turbine blade consists of each wing section, and the performance of the wing section is also directly related to the performance of the hydraulic turbine.

Therefore, priority is given to optimizing the wing section to improve the hydrodynamic performance of the airfoil.

Airfoil design is a key element of hydraulic turbine design, and only by choosing a suitable airfoil can the efficiency of a hydraulic turbine be maximized [5]. The commonly used airfoil design methods in the early days can be categorized into two types: the forward design approach and the backward design approach. The forward design approach often uses mathematical equations to determine the shape of the airfoil first, followed by experimental measurements. However, there is a large uncertainty as to whether the flow characteristics and hydrodynamic performance of a new airfoil designed using this method are as expected. The inverse design method is usually based on the surface pressure coefficients or velocity distributions of a given airfoil, and numerical simulations using computational fluid dynamics are utilized for continuously adjust airfoil geometry to approximate the desired hydrodynamic features. With rapid development of computers and numerical optimization methods, an optimization method that integrates computational fluid dynamics with optimization algorithms

* Corresponding author.

† These authors have the same contribution to this article.

has begun to receive widespread attention and has gradually become a major trend in airfoil optimization [6].

In the blade design of a hydraulic turbine, the distribution of airfoil shape, airfoil spread, chord length distributed along the spreading direction, thickness and torsion angle as critical influencing factors [7]. To increase the efficiency of hydraulic turbines, scholars have conducted relevant studies. Wu et al. [8] adopted the Schmitz theory to design blades and fully considered the impact of wing tip loss and airfoil loss on the efficiency of the hydraulic turbine. Abolfazl et al. [9] used a continuous genetic algorithm and binary genetic algorithm, respectively, and optimized the blades with the chord length and the distribution of torsion as the design variables. Continuous genetic algorithm is superior than the binary genetic algorithm in terms of accuracy and computation time. Zhang et al. [10] compared the angles of attack and lift-to-drag ratios of multiple airfoils by optimizing a multi-island genetic algorithm, which in turn led to the conclusion of which airfoil was more effective in gaining energy. Lee and Shin [11] optimized the cross-section design of the initial blade at several locations based on genetic algorithm, and the optimized blade became lighter, which also reduces the applied loads of the wind turbine. Grasso [12] used a scheme to find the optimum by combining the genetic algorithm and gradient class algorithm and finally obtained airfoils with the high aerodynamic performance of the airfoil. He and Agarwal [13] optimized the S809 airfoil using MOGA with the optimization goals of increasing lift and lift-to-drag ratio, and the outcome indicates that the optimized wing shows dramatic improvement in both lift coefficient and lift-to-drag ratio compared to the original S809 airfoil. Chern et al. combined genetic algorithms with the direct force immersed boundary approach for the optimization of the blade, and the efficiency of the optimized wind turbine blade designed in such an approach increased by 5.61% compared with that of the original blade by 5.61%. Yeo et al. [15] combined a genetic algorithm and Blade Momentum Theory (BEM) to optimize the blade for the objective of local torsion angle and chord length. The performance of the optimized BEM model was compared with the experiments, thus verifying the accuracy of the optimized BEM model. Landa Couto et al. [16] used the blade mass, largest tip displacement, the vibration intrinsic frequency, and the crucial load coefficient as the target function to optimize the blade structure. The structure of the wind turbine blade was optimized and all the optimized blade structures were significantly improved. Pholdee et al. [17] used the torsion angle on the blade radius and the position of the rotational axis on the blade chord length as the design variables, and power factor maximization was taken as the optimization objective. The best blade achieved in this study shows improved behavior over the initial blade under low wind velocity conditions with a wind speed of 10 m/s.

In this article, the tidal current energy horizontal axis hydraulic turbine blade airfoil is treated as an object of study, and the Class Shape Function Transformation (CST) parameterization method is used to parameterize the airfoil, which takes the lift coefficient and lift-to-drag ratio under several working situations as the optimization objectives. To find the global optimal solution, a multi-island genetic approach is to solving the model, and the hydrodynamic performance

and pressure coefficients are obtained through the XFOIL software, with the final goal of obtaining a compliant airfoil. The various modules of the optimization are integrated into the iSight platform to run automatically. Finally, the airfoils under different design conditions are analyzed to obtain the characteristics of various types of airfoils, which provides a basis for carrying out hydraulic turbine design.

2. Airfoil parameterization

2.1. Parametric modeling of airfoil

The airfoils at different locations of the horizontal axis turbine blade spread have different design requirements [18]. The airfoil at the tip does not need to bear large loads, so the thickness of the airfoil here is usually designed to be small. The tip is the key area to capture energy, so the lift resistance in this area is relatively high; the middle part of the blade is the transition zone, and the airfoil cross-section is designed with a smooth transition. The root of the blade requires greater structural strength, so the thickness of the design is larger at this location.

From the consideration of hydrodynamic and structural characteristics, the hydraulic turbine blade needs different airfoils for stacking modeling along its spreading direction. Generally, each part is considered as follows:

- (1) Blade tip (75%–100% of blade spread): The blade tip is the key area of the hydraulic turbine to gain energy. Here the thickness of the airfoil design is small. In order to obtain better hydrodynamic performance, as well as a larger lift-to-drag ratio and better stall characteristics, its maximum relative thickness is generally not more than 20%.
- (2) In the design of the middle blade airfoil of the hydraulic turbine, it is necessary to consider the transition smoothness with the trail and tip of the blade, and its geometrical characteristics need to have better geometrical compatibility (at the position of 30%–75% of the blade spreading), and its maximal relative thickness is generally between 21%–28%.
- (3) During the actual operation of the hydraulic turbine, the incoming flow will continuously impact the blade. Therefore, the root part of the blade requires high fatigue strength and good structural characteristics. The hydraulic turbine is thicker at the trail part of the blade (at 0%–30% of the blade spread), and the maximum relative thickness is generally above 28%. For large-scale tidal current energy turbine blades, the maximum relative thickness can be designed to be more than 40%.

In conclusion, in order to have a better energy-yielding efficiency of the turbine, the selected airfoil needs to get a larger lift-to-drag ratio.

In this paper, the selected turbine airfoil is from the literature [19], and the surface of the turbine blade is made by the “Ten-Section Method”, a complete blade is divided into ten different cross-sections and then connected with curves in a smooth transition, and the parameters of its various cross sections are shown in Table 1. The hydraulic turbine model is shown in Fig. 1. To meet the NACA638-XX

Table 1
Airfoils at each spreading direction of the turbine

| Serial number | NACA | r (mm) | c (r) | c (mm) | t/c (%) | t (mm) | β (°) |
|---------------|-------|--------|--------|--------|---------|--------|-------|
| 1 | 63858 | 60 | 0.0483 | 29 | 58 | 16.87 | 23 |
| 2 | 63825 | 120 | 0.1117 | 67 | 25 | 16.75 | 19 |
| 3 | 63823 | 180 | 0.1109 | 66.56 | 22.8 | 15.51 | 12.35 |
| 4 | 63822 | 240 | 0.1045 | 62.72 | 21.9 | 13.73 | 9.96 |
| 5 | 63820 | 300 | 0.0988 | 59.3 | 20.05 | 12.07 | 8.91 |
| 6 | 63819 | 360 | 0.0932 | 55.92 | 18.80 | 10.51 | 8 |
| 7 | 63817 | 420 | 0.0883 | 52.98 | 17.15 | 9.14 | 7.03 |
| 8 | 63816 | 480 | 0.0857 | 51.44 | 16.1 | 8.08 | 6.21 |
| 9 | 63815 | 540 | 0.0830 | 49.82 | 15.1 | 7.05 | 5.74 |
| 10 | 63813 | 600 | 0.0733 | 44 | 12.8 | 5.54 | 5.5 |

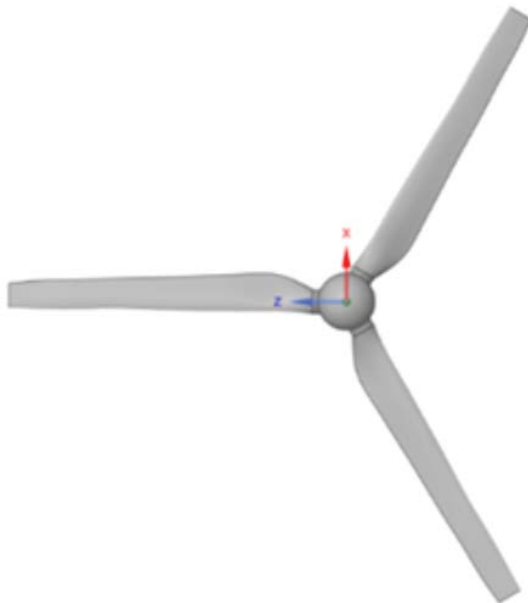


Fig. 1. Three-dimensional model of a tidal turbine.

series of airfoils in the water for better energy acquisition, it is necessary to carry out some optimization. Now the airfoils at 8, 9, and 10 are optimized to increase the maximum lift-to-drag ratio. The relative thicknesses of these airfoils are 16%, 15% and 13%, respectively. In Table 1, r is the paddle radius; c is the chord distance; t is the thickness and β is the torsion angle.

2.2. Parametric modeling of airfoil

The CST parameterization method was first proposed by Kou et al. [20] at the 11th AIAA/SSMO Multidisciplinary Analysis and Optimization Conference in 2006. The airfoil geometry is described by introducing a Class Function and a Shape Function. The Class Function serves to specify the basic contour of the airfoil, for example, it specifies: a rounded tip and tail airfoil, an elliptical airfoil with a rounded tip and tail, and a wing with a pointed tip and tail. The shape function is to adjust the basic airfoil contour, adjusting

the airfoil leading edge and airfoil trailing edge through some parameter points to achieve the design desired shape.

The mathematical expression of CST parametric method is:

$$\frac{y}{b} \left(\frac{x}{b} \right) = C \left(\frac{x}{b} \right) \cdot S \left(\frac{x}{b} \right) + \frac{x}{b} \cdot \frac{\Delta y_{TE}}{b} \tag{1}$$

where Δy_{TE} is thickness of the trailing edge of the airfoil; C(x/b) is category function, and S(x/b) is shape function.

The mathematical representation of the category function is given by:

$$C \left(\frac{x}{b} \right) = \left(\frac{x}{b} \right)^{N_1} \cdot \left(1 - \frac{x}{b} \right)^{N_2} \tag{2}$$

where N₁, N₂ are control coefficients.

When N₁ and N₂ take different values, different geometries can be defined. When N₁ and N₂ take different values, different geometries can be defined. By taking S(x/b) value of 1, by taking Δy_{TE} value of 0, Eq. (1) can be simplified to:

$$\frac{y}{b} \left(\frac{x}{b} \right) = C \left(\frac{x}{b} \right) = \left(\frac{x}{b} \right)^{N_1} \cdot \left(1 - \frac{x}{b} \right)^{N_2} \tag{3}$$

Taking different values for N₁ and N₂, respectively, different wing profiles are obtained as shown in Fig. 2:

When N₁ = 0.5, N₂ = 1, it corresponds to the NACA series of round-head and pointed-tail airfoils; when N₁ = 0.5, N₂ = 0.5, it corresponds to the elliptical airfoils with round heads and round tails; and when N₁ = 1, N₂ = 1, it corresponds to the airfoils with pointed heads and pointed tails.

In this paper, the mathematical representation of the category function corresponding to N₁ = 0.5, N₂ = 1 is chosen as:

$$C \left(\frac{x}{b} \right) = \sqrt{\frac{x}{b} \left(1 - \frac{x}{b} \right)} \tag{4}$$

The first term $\sqrt{x/b}$ on the right-hand side of the above equation can be used to ensure that the profile near

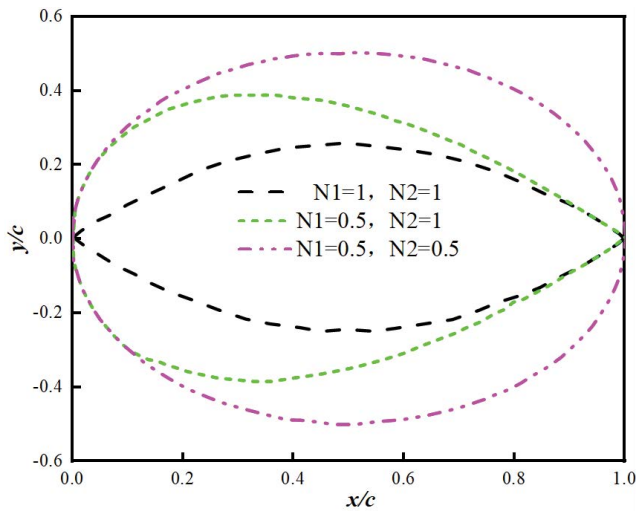


Fig. 2. Geometries grown with different values of N_1, N_2 .

the front edge of the airfoil has a rounded shape, whereas the second term $(1 - x/b)$ can be used to ensure that the profile near the trailing edge of the airfoil has a pointed shape, which corresponds exactly to an airfoil with a rounded tip and pointed tail.

3. Optimizing problem parameters

The ultimate goal of this paper is to design an airfoil that can meet the operating properties of horizontal axis tidal current turbine blades under complex operating conditions. Therefore, the geometrical characteristics and hydrodynamic performance of the airfoil need to refer to the multi-operating conditions of the horizontal axis tidal energy turbine. In order to meet the above conditions, the following elements are optimized: (1) constraint function f_x and (2) optimization conditions.

3.1. Constraint function

The performance requirements of hydraulic turbine airfoils are very complicated, and the focuses of different airfoil designs on each performance parameter are different and sometimes even contradictory to each other, whereas multi-objective optimization can weigh and allocate each performance parameter to get the airfoil with the best overall behavior. When the floater goes in motion in hydrostatic water, the structural motion generates radiation. It is worth noting that these forces are a function of the motion of the structure. Where mass and drag coefficients are taken into account in the dynamic equations [21]. The optimization process not only needs to consider the hydrodynamic behavior of the airfoil such as lift-to-drag ratio, but also needs to consider the hydrodynamic stability of the airfoil in the stall region, and the stability parameters are defined as follows:

The largest relevant thickness of the original bionic airfoil is specified as h_0 . Constraints can be imposed in order not to change in the shape of the optimized airfoil geometry:

$$12.5\% \leq \frac{t}{c} = h_0 \leq 16.5\% \quad (5)$$

where t is the maximum thickness considered for the corresponding airfoil.

In general, the location of the maximum thickness of the optimized airfoil at 8, 9, and 10 is at 35% chord length from the forefront, and the constraint function can be set in order to optimize the airfoil without changing the airfoil geometry too much [22]:

$$32\% \leq \frac{h_t}{c} \leq 37\% \quad (6)$$

where h_t is the distance from the forefront where the maximum thickness of the bionic airfoil is located.

For 2D airfoils, increasing the curvature at appropriate locations can raise the lift-to-drag ratio, however, too much curvature will affect the overall blade intensity. Parallelism between the optimized airfoil and the initial airfoil should also be given consideration. It is therefore possible to limit the combination of the three factors:

$$3\% \leq \frac{w}{c} \leq 5\% \quad (7)$$

where w is the airfoil curvature.

The position of the bend is appropriately shifted towards the trailing edge to favor the maximum lift-to-drag ratio of the tidal energy turbine airfoil, and the constraints are imposed in a way that ensures geometrical similarity:

$$45\% \leq \frac{w_f}{c} \leq 55\% \quad (8)$$

where w_f is the distance from the placement at the maximum bending at the front edge of the wing.

Most of the noise generated during the operation of a tidal energy turbine originates from the eddy currents generated by the motor and the blades. The vortices generated by the blades in turn mostly originate from the tip vortices. Thus, the noise reduction treatment of hydraulic turbines can be realized by improving the thickness of the wing trailing edge at the blade tip. Previous studies have shown that the greater the thickness of the airfoil trailer edge, the greater the noise generated by the airfoil's trailing edge. However, the thickness of the wing trailing edge is not convenient for processing when it is too small, so the comprehensive consideration of the thickness of the wing trailing edge can be designed as:

$$y_{u,1} - y_{l,1} \leq 0.01 \quad (9)$$

where $y_{u,1}$ is the y-coordinate of the upper airfoil surface, and $y_{l,1}$ is the y-coordinate of the undersurface of an airfoil.

For airfoils of different thicknesses, the weights of each parameter in the airfoil design process are not fixed values and need to be adjusted according to different performance requirements because of the different emphasis on airfoil performance at different locations. Finally, the multi-objective function can be expressed as:

$$f = 0.15h + 0.25h_1 + 0.1w_i + 0.35w_i + 0.15\Delta y \quad (10)$$

where h is the maximum relative thickness of the initial bionic wing; h_1 is the maximum thickness is located at a distance from the leading edge; w_1 is curvature; w_2 is the location of the maximum bend is the distance from the leading edge, and Δy is airfoil trailing edge.

3.2. Optimization conditions

The lift-to-drag ratio C_l/C_d , drag coefficient C_d and the maximum thickness T_m of the wing with an angle of attack of 5° are selected as the optimization target parameters, as shown in Table 2, where $C_l/C_d > (C_l/C_d)_0$, C_{d0} and T_{m0} denotes the initial airfoil type corresponding to the reference airfoil type. In this paper, NACA63813, 63815 and 63816 airfoils of the same thickness as the target airfoils are selected as reference airfoils. The optimization condition in the design process is that the lift-to-drag characteristic of the designed airfoil is better than the reference airfoil of the same thickness.

4. Numerical methods and optimization algorithms

4.1. Numerical method

The lift-to-drag characteristics of the airfoil originate from two parts in the incoming flow: firstly, when the incoming flow passes through the airfoil, the lower surface is in the positive pressure region and the upper surface is in the negative pressure region, which creates a pressure difference between the two, and secondly, the viscous effect generated on the surface of the airfoil. Influence of viscosity on drag coefficient is larger than that on the lift coefficient, and the effect decreases with increase of the angle of attack. The Reynolds number is used as a measure of the relative size of the inertial force and the viscous force, and the influence of the viscous force is more remarkable when the Reynolds number is smaller. An appropriate increase in Reynolds number can reduce the drag coefficient.

$$Re = \frac{Vl}{\nu} \tag{11}$$

where, V is the flow rate; l is the characteristic length, and ν is the kinematic viscosity. The Reynolds number was set to $Re = 1 \times 10^6$.

To ensure the optimization process and validation are accurate, the effects of the mesh itself on the outcome are excluded. The grid-independence is shown in Fig. 3, and the lift coefficient of the NACA63816 airfoil is used as the convergence criterion. The results show that as the number of meshes grows to 200,000, the lift coefficient for C_l is 1.31.

Table 2
Optimization parameters

| Optimization conditions | Weights | Parameters | Optimum |
|-------------------------|---------|------------|-----------------------------|
| Lift-to-drag ratio | 0.2 | C_l/C_d | $C_l/C_d > (C_l/C_d)_0$ |
| Drag | 0.2 | C_d | $C_d \leq C_{d0}$ |
| Maximum thickness | 0.7 | T_m | $[T_m - T_{m0}] \leq 0.001$ |

As the number of meshes is growing, the lift coefficient stays constant. In this case, it can be assumed that the calculation outcome is irrelevant to the number of grids. A grid of 200,000 is used in the subsequent studies of this paper.

XFOIL software is used to numerically predict the lift resistance and other characteristics of the airfoil and compared with Fluent software, which is widely used in the optimization of airfoil design owe to the benefits of its rapid solution and good stability. Fig. 4 shows the results of numerical simulation and XFOIL calculation for the NACA63816 airfoil with different angles of attack. The reasons for choosing to compare the results with those of XFOIL are: (1) XFOIL has high computational accuracy, and (2) it is easy to modify the parameters of XFOIL, due to the lack of experimental link for the working conditions of the numerical simulation in the thesis, the method used

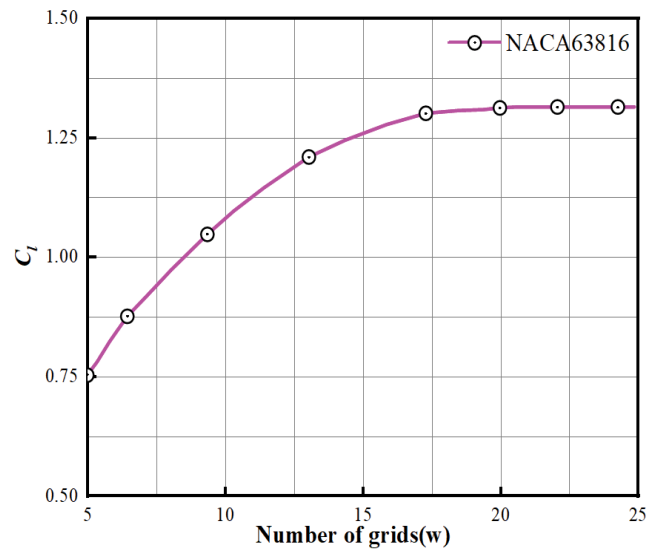


Fig. 3. Grid independence verification.

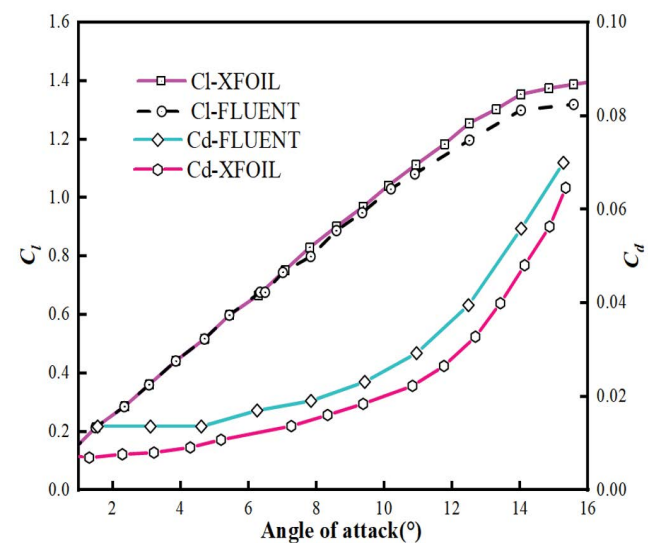


Fig. 4. Calculation accuracy test.

in this study compares the results of numerical simulation with those of XFOIL under the same working conditions. XFOIL under the same working conditions to determine its accuracy by comparing the results obtained from numerical simulation. From the figure, which shows that the angle of attack before reaching the stall angle of attack, the numerical simulation and XFOIL results are basically in agreement, and after the stall, the results show errors, but the changes are basically consistent.

5. Optimization and result analysis

5.1. Optimization of the design process

Using iSight software, the airfoil generated by the CST module of the airfoil parameterization module is imported into the XFOIL module to solve the airfoil, and the results are outputted, followed by the output of the target parameters by the Function module of the computational function module, and then optimized by the Multi-Island Genetic Algorithm (MIGA) in the Optimization module, as shown in Table 3 of the iSight software. By batch processing the output results, comparing the parameters before and after the wing optimization, and repeating the above operation until the optimal solution is obtained, the operation flow is shown in Fig. 5.

5.2. Optimization results

Fig. 6 shows the comparison of the shape of NACA63816/15/13 airfoils after optimization by iSight software, it can be found that the geometry of the three

optimized airfoils is shifted upward as a whole compared with the initial airfoil. Figs. 7 and 8 show the comparison of the lift coefficient and lift-to-drag ratio of the airfoils before and after optimization. It can be observed that the previous lift coefficient and after optimization grows linearly in the range of the angle of attack from -5° to 5° and the growth rate is larger. the growth of the lift coefficient from 5° to 15° is slow and non-linear, and the lift coefficient starts to decrease after 15° when it gradually reaches the stall region. This is because, for NACA6xx series airfoils, the airfoil's coefficient of lift increases with increasing angle of attack over a given range, but the lift coefficient is faster than the drag coefficient, and the lift-to-drag ratio increases gradually; when the angle of attack becomes 5° , the lift-to-drag ratio decreases rapidly because the drag coefficient increases rapidly at this time and the lift coefficient is growing slowly. From the comparison of the optimized airfoils, it can be found that the lift coefficients of NACA63816/15/13 have increased by 20%/15%/14% at 5° , and the drag ratios have increased by 28%/16%/14%, respectively.

Figs. 9 and 10 show the vortex streamline diagrams and pressure cloud diagrams of the airfoil before and after

Table 3
Control parameters of multi-island genetic algorithm

| Parameter name | Parameter settings |
|-----------------------------------|--------------------|
| Subspecies group size | 7 |
| Number of subspecies archipelagos | 8 |
| Evolutionary algebra | 50 |
| Probability of hybridization | 0.96 |
| Probability of mutation | 0.02 |
| Mobility | 0.02 |
| Migration interval | 6 |

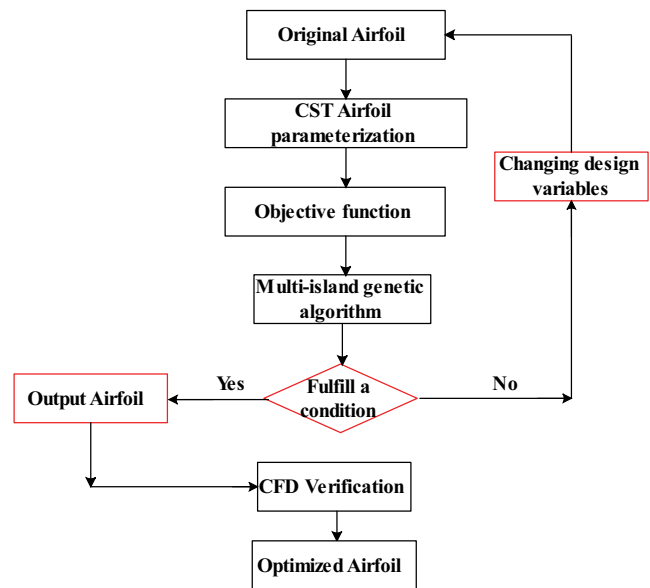


Fig. 5. Optimization process.

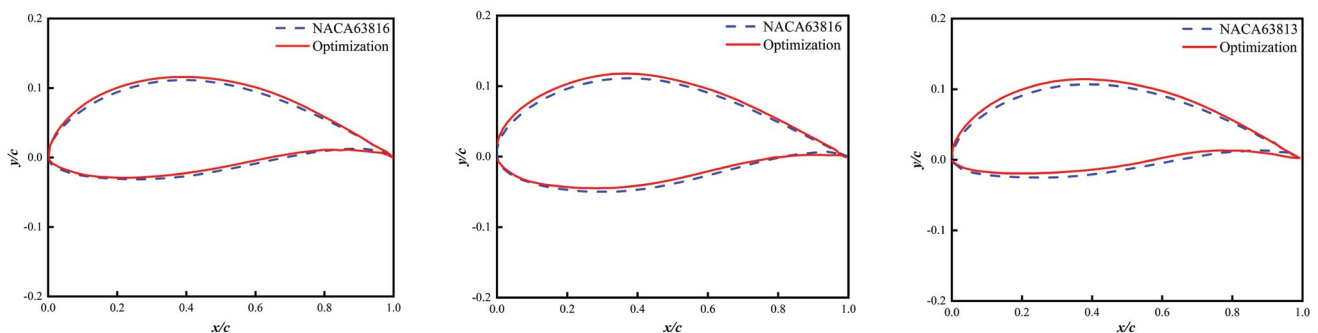


Fig. 6. Comparison of NACA63816/63815/63813 airfoil optimization.

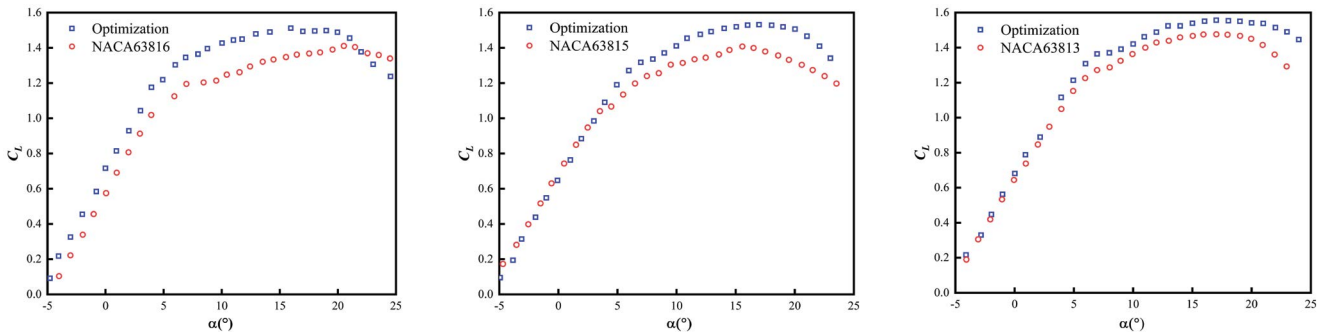


Fig. 7. Optimized lift ratio of NACA63816/63815/63813 airfoil.

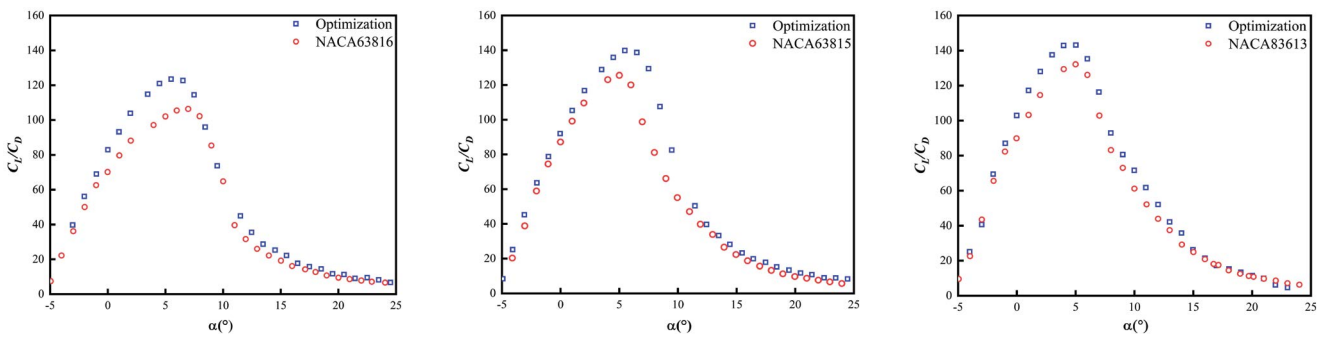


Fig. 8. Optimized lift-to-drag ratio of NACA63816/63815/63813 airfoil.

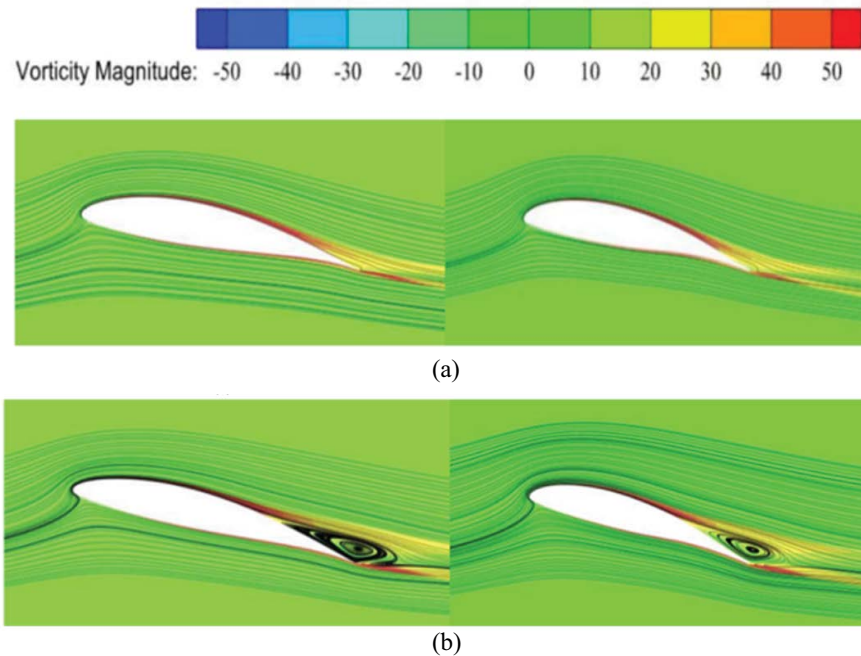


Fig. 9. NACA63813 airfoil vortex streamline. Angle of (a) attack 10° and (b) attack 15° (initial airfoil on the left, optimized airfoil on the right).

NACA63813 optimization. Comparing the velocity streamlines diagrams before and after optimization, it can be seen that as the range of negative pressure area of the airfoil becomes larger after optimization, which results in an

increase in the flow velocity over the upper surface and the area becomes larger, which also means that the efficiency of the turbine blade will be increased in the actual working process. Observing the pressure cloud after optimization,

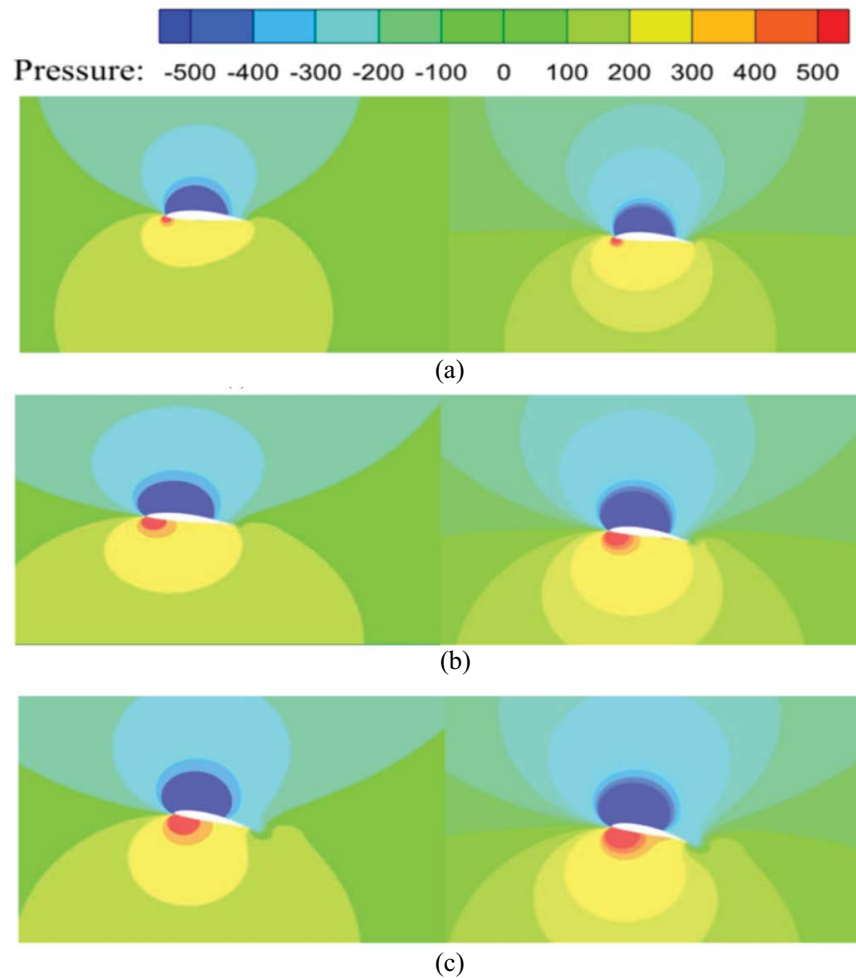


Fig. 10. NACA63813 airfoil pressure cloud. Angle of (a) attack 5° , (b) attack 10° , and (c) attack 15° (initial airfoil on the left, optimized airfoil on the right).

which shows that when the curvature and thickness of the airfoil are increased and shifted backward with respect to the maximum curvature and thickness, the flow velocity of water on the upper surface of the airfoil will be larger, and then the suction force on the lower surface of the airfoil will increase, which will finally make the coefficient of lift and the coefficient of lift-to-drag ratio larger. From the pressure cloud diagrams before and after the airfoil optimization, as can be seen that the negative pressure area of the upper airfoil surface is wider and more uniform. The initial airfoil's negative pressure zone is focused in the forward zone of the airfoil, while the optimized airfoil's negative pressure zone is focused in the middle zone of the forward part of the airfoil. The negative pressure zone is more evenly distributed, which means that the optimized wing has better structural stability.

6. Numerical simulation of turbine

The optimized hydraulic turbine is modeled and the flow domain is divided. The entire turbine flow field domain is divided into two regions. The rotating domain containing

the turbine model and the stationary domain outside the turbine. In Fig. 11, the inlet of the flow field domain is $6D$ from the turbine, the upper, lower, left, and right walls are $6D$ from the turbine, and the outlet is $24D$ from the turbine. The inlet boundary of the calculation field is given as a velocity inlet with an inlet velocity of 1.0 m/s, the turbulence intensity is set to 5% , and the hydrodynamic diameter is $12D$. The direction of the inflow is perpendicular to the velocity inlet, and it is a uniform incoming flow. The downstream outlet is defined as the pressure outlet boundary condition, and the outlet pressure is the default value. The top, bottom, left, and right walls of the static domain are free-slip walls. The turbine rotation speed is set to 85 rpm, and the turbine walls are given as no-slip walls. The pressure-velocity coupled solver uses the commonly used SIMPLEC algorithm, with the first-order inverse distinct hidden format for the time term, the second-order windward for the spatial discretization of the pressure term, and the first-order windward format for the discretization of the momentum term, where the default settings are used for each value. The turbulence model is the $SSTk-\omega$ model, which has greater computational accuracy for smaller tip speed ratios. Where k stands

for the turbulent kinetic energy and ϵ stands for the dissipation rate of this energy. The solver is the transient solver with time steps taken to rotate the turbine by $1^\circ:0.0019379845$ s. The thrust torque of the turbine is also monitored.

The pressure cloud diagram of the hydraulic turbine is illustrated above in Fig. 12, and the pressure cloud diagram above and below the blade can be divided into pressure surface and suction surface, with the pressure surface being the positive pressure area and the suction surface being the negative pressure zone. From the figure, it is clear that the pressure minimum position of the hydraulic turbine blade is at leading edge of the blade tip in the suction part, and the maximum pressure is situated at the front edge of the blade tip in the positive pressure zone. The pressure difference between the positive pressure zone and the negative pressure zone causes turbine blade to generate a lift force, which then forms a torque acting on the blade to make the turbine rotate and output power to the outside.

From Table 4, as can be observed that the grid number levels of the hydraulic turbine converge gradually at 3 and 4 and are close to the actual thrust. Since the computational efficiency will be reduced when the number of grids is too large, the subsequent calculation of various indexes of the hydraulic turbine model before and after optimization is numerically calculated using grid 3. From Fig. 13, as can be

observed that the C_p and C_z of the hydraulic turbine after optimization are larger than those before optimization at different TSRs, where the difference in C_p value is the largest at TSR = 5, and the efficiency improvement is 6.34%. The change trend of the C_z value is smaller after TSR = 7.

When the turbine speed is fixed, as can be observed from the TSR and power coefficient curves in Fig. 13 that when the TSR is small, the turbine power is smaller. This is due to the angle of attack of the blades becomes larger gradually from the increase of the incoming flow rate, so the flow field on the surface near the blades starts to have boundary layer separation, which further causes the airfoil to stall and form a vortex to fall into the wake field, which results in the

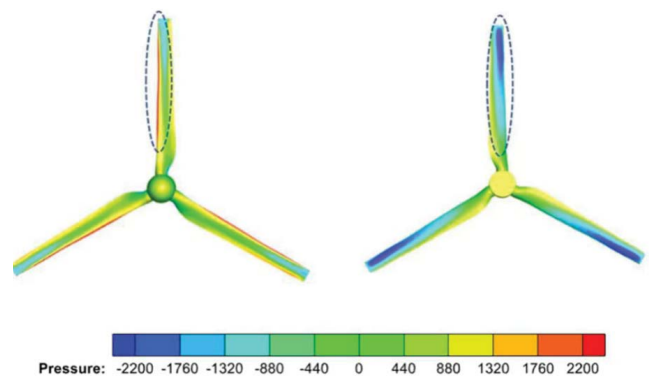


Fig. 12. Turbine surface pressure cloud.

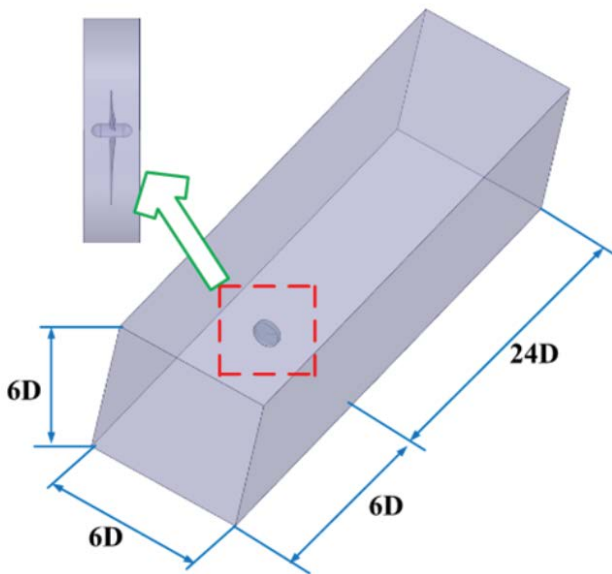


Fig. 11. Turbine computational domain.

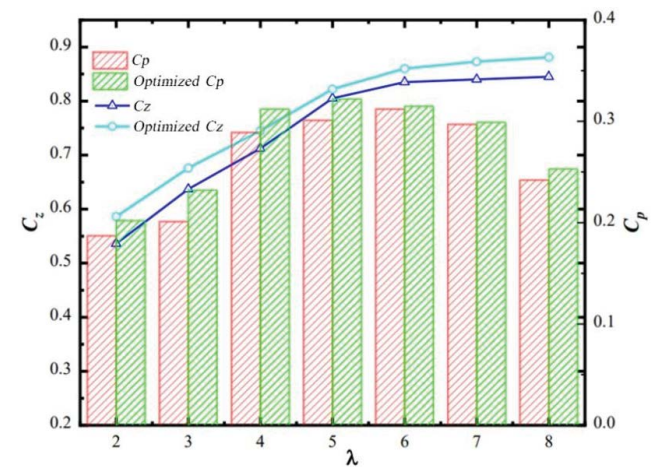


Fig. 13. Comparison of C_p and C_z after turbine optimization.

Table 4
Number of turbine grids

| Grid sequence | Grid before optimization (million) | Optimized grid (million) | Before optimization thrust (N) | After optimization thrust (N) | Actual thrust (N) |
|---------------|------------------------------------|--------------------------|--------------------------------|-------------------------------|-------------------|
| 1 | 160 | 161 | 342.5 | 351.5 | |
| 2 | 244 | 245 | 348.1 | 368.7 | |
| 3 | 338 | 341 | 356.3 | 380.8 | 350 |
| 4 | 451 | 456 | 356.8 | 380.5 | |

fluctuation of the lift of the blades and superposition with the turbine rotation, thus leading to a smaller efficiency of the turbine in the field of the energy gained. When the TSR gradually becomes larger, the turbine energy acquisition efficiency gradually increases. As the TSR is too large, the smaller incoming velocity results in reduction of the wing angle of attack, the blade lift decreases, and the turbine efficiency gradually becomes smaller.

7. Conclusion

The NACA63816/15/13 airfoils were parameterized by the CST method to optimize the airfoils along the turbine blades at the position of 75%–100% of the spread, so as to increase the overall energy gain of the turbine. The major findings are that:

- (1) Using multi-island genetic algorithm, the maximum lift-to-drag ratio and lift coefficient at 5° are optimized as the objective function. The findings indicate that the overall lift coefficient and lift-to-drag ratio of the optimized airfoil are larger than those of the initial airfoil.
- (2) The lift coefficients of the optimized NACA63816/15/13 airfoils at 5° increased by 20%/15%/14% and the lift-to-drag ratios risen by 28%/16%/14%, respectively. The optimized lower airfoil has an overall larger pressure coefficient and the lift coefficient of the upper airfoil becomes smaller, and the airfoil obtains a better aerodynamic effect.
- (3) The negative pressure zone of initial airfoil is focused on forward region, while negative pressure zone of optimized airfoil is focused on the forward-middle region, and distribution of the negative pressure zone is more homogeneous, which means that the optimized airfoil structure is more stable.

Funding

This study was funded by the National Key Research and Development Program of China “Cooperative Study on Comprehensive Evaluation Methods of Wave and Tidal Currents Energy Technology” (No. 2019YFE0102500), National Natural Science Foundation of China (Nos. 52001138 and 52101356), National Natural Science Foundation of Jiangsu Province (No. BK20201029), and Basic Science (Natural Science) Program of Colleges and Universities in Jiangsu Province (No. 21KJB580011). In addition, it was funded by the Key R&D Program of Lianyungang City (No. CG2224) and the Natural Science Practice Program for Graduate Students of Jiangsu Province (No. SJCX23_1817).

References

- [1] M.L. Cai, Y.X. Wang, Z.X. Jiao, Y. Shi, Review of fluid and control technology of hydraulic wind turbines, *Front. Mech. Eng.*, 12 (2017) 312–320.
- [2] Z.Y. Zhang, X.Y. Chen, H.T. Wu, W.X. Liu, L. Cui, Numerical study of a novel hybrid system with the Wavestar wave energy converter array and a SPIC semi-submersible floating platform, *J. Cleaner Prod.*, 407 (2023) 137178, doi: 10.1016/j.jclepro.2023.137178.
- [3] Z.Y. Zhang, F.M.A. Altalbawy, M. Al-Bahrani, Y. Riadi, Regret-based multi-objective optimization of carbon capture facility in CHP-based microgrid with carbon dioxide cycling, *J. Cleaner Prod.*, 384 (2023) 135632, doi: 10.1016/j.jclepro.2022.135632.
- [4] W.X. Liu, L. Liu, H.T. Wu, Y.L. Chen, X.B. Zheng, N.Y. Li, Z.Y. Zhang, Performance analysis and offshore applications of the diffuser augmented tidal turbines, *Ships Offshore Struct.*, 18 (2023) 68–77.
- [5] T. Wilberforce, Z. El Hassan, A. Durrant, J. Thompson, B. Soudan, A.G. Olabi, Overview of ocean power technology, *Energy*, 175 (2019) 165–181.
- [6] X.J. Sun, D.G. Huang, An explosive growth of wind power in China, *Int. J. Green Energy*, 11 (2014) 849–860.
- [7] L. Zhang, S.-q. Wang, Q.-h. Sheng, F.-m. Jing, Y. Ma, The effects of surge motion of the floating platform on hydrodynamics performance of horizontal-axis tidal current turbine, *Renewable Energy*, 74 (2015) 796–802.
- [8] B.G. Wu, X.M. Zhang, J.M. Chen, M.Q. Xu, S.X. Li, G.Z. Li, Design of high-efficient and universally applicable blades of tidal stream turbine, *Energy*, 60 (2013) 187–194.
- [9] P. Abolfazl, D. Maziar, R. Saeed, Genetic algorithms for the design and optimization of horizontal axis wind turbine (HAWT) blades: a continuous approach or a binary one?, *Sustainable Energy Technol. Assess.*, 44 (2021) 101022, doi: 10.1016/j.seta.2021.101022.
- [10] Z.Y. Zhang, B. Wu, L.Y. Wu, W.X. Liu, L. Liu, N.Y. Li, L. Cui, Optimization of the bionic wing shape of tidal turbines using multi-island genetic algorithm, *Machines*, 11 (2023) 43, doi: 10.3390/machines11010043.
- [11] S.-L. Lee, S.J. Shin, Structural design optimization of a wind turbine blade using the genetic algorithm, *Eng. Optim.*, 54 (2022) 2053–2070.
- [12] F. Grasso, Hybrid Optimization for Wind Turbine Thick Airfoils, Collection of Technical Papers - AIAA/ASME/ASCE/AHS/ASC Structures, Structural Dynamics and Materials Conference, 53rd AIAA/ASME/ASCE/AHS/ASC Structures, Structural Dynamics and Materials Conference 20th AIAA/ASME/AHS Adaptive Structures Conference 14th AIAA, 2013, doi: 10.2514/6.2012-1354.
- [13] Y.L. He, R.K. Agarwal, Shape optimization of NREL S809 airfoil for wind turbine blades using a multi-objective genetic algorithm, *Int. J. Aerosp. Eng.*, 2014 (2014) 864210, doi: 10.1155/2014/864210.
- [14] M.-J. Chern, D.G. Tewolde, C.-C. Kao, N. Vaziri, Vertical-axis wind turbine blade-shape optimization using a genetic algorithm and direct-forcing immersed boundary method, *J. Energy Eng.*, 147 (2021) 04020091, doi: 10.1061/(ASCE)EY.1943-7897.0000741.
- [15] E.J. Yeo, D.M. Kennedy, F. O'Rourke, Tidal Current Turbine Blade Optimisation Using a Combined Genetic Algorithm-Blade Element Momentum Theory Model, The 33rd International Conference on Efficiency, Cost, Optimization, Simulation and Environmental Impact of Energy Systems, 2020.
- [16] L. de Landa Couto, N.E. Moreira, J.Y. de Oliveira Saito, P.H. Hallak, A.C. de Castro Lemonge, Multi-objective structural optimization of a composite wind turbine blade considering natural frequencies of vibration and global stability, *Energies*, 16 (2023) 3363, doi: 10.3390/en16083363.
- [17] N. Pholdee, S. Bureerat, W. Nuantong, Kriging surrogate-based genetic algorithm optimization for blade design of a horizontal axis wind turbine, *CMES-Comp. Model. Eng. Sci.*, 126 (2021) 261–273.
- [18] M. Ahmad, A. Shahzad, F. Akram, F. Ahmad, S.I. Ali Shah, Design optimization of Double-Darrieus hybrid vertical axis wind turbine, *Ocean Eng.*, 254 (2022) 111171, doi: 10.1016/j.oceaneng.2022.111171.
- [19] G.S. Payne, T. Stallard, R. Martinez, Design and manufacture of a bed supported tidal turbine model for blade and shaft load measurement in turbulent flow and waves, *Renewable Energy*, 107 (2017) 312–326.
- [20] J.Q. Kou, L. Botero-Bolívar, R. Ballano, O. Marino, L. de Santana, E. Valero, E. Ferrer, Aeroacoustic airfoil shape optimization

- enhanced by autoencoders, *Expert Syst. Appl.*, 217 (2023) 119513, doi: 10.1016/j.eswa.2023.119513.
- [21] Z.Y. Zhang, M.H. Du, Y.K. Li, W.X. Liu, H.T. Wu, L. Cui, Z.H. Yan, X. Wang, Q.M. Liao, M. Li, Effects of mooring configuration on the dynamic behavior of a TLP with tendon failure, *Desal. Water Treat.*, 268 (2022) 215–228.
- [22] R.J. Balamurugan, H.A.Z. Al-Bonsrulah, V. Raja, K. Lokeshkumar, S.D. Kannan, M. Senthil Kumar, R. Rasheed, P. Rajendran, M. Al-Bahrani, Design and multiperspectivity-based performance investigations of H-Darrieus vertical axis wind turbine through computational fluid dynamics adopted with moving reference frame approaches, *Int. J. Low-Carbon Technol.*, 17 (2022) 784–806.